Computer Assisted Radiology and Surgery manuscript No.
(will be inserted by the editor)

Multiple CT-Reconstructions for Locally Adaptive Anisotropic Wavelet Denoising

Anja Borsdorf[1], Rainer Raupach[2], Joachim Hornegger[1]

[1] Institute of Pattern Recognition, Friedrich-Alexander-University Erlangen-Nuremberg, Germany
[2] Siemens Medical Solutions, Forchheim, Germany

Received: date / Revised version: date

Abstract *Objective* The signal-to-noise ratio in computed tomography (CT) data should be improved by using adaptive noise estimation for level-dependent threshold determination in the wavelet domain.
Method The projection data measured in CT and, thus, the slices reconstructed from these data are noisy. For a reliable diagnosis and subsequent image processing, like segmentation, the ratio between relevant tissue contrasts and the noise amplitude must be sufficiently large. By separate reconstructions from disjoint subsets of projections, e.g. even and odd numbered projections, two CT volumes can be computed, which only differ with respect to noise. We show that these images allow a position and orientation adaptive noise estimation for level-dependent threshold determination in the wavelet domain. The computed thresholds are applied to the averaged wavelet coefficients of the input data.
Results The final result contains data from the complete set of projections, but shows approximately 50% improvement in signal-to-noise ratio.
Conclusions The proposed noise reduction method adapts itself to the noise power in the images and allows for the reduction of spatially varying and oriented noise.

1 Introduction

In computed tomography (CT), the projections acquired at the detector are noisy, predominantly caused by quantum statistics. This noise propagates through the reconstruction algorithm to the reconstructed slices. Pixel noise in the images can be reduced by increasing the radiation dose or by choosing a smoothing reconstruction [14]. However, with respect to patients' care, the least possible radiation dose is required and a smoothing reconstruction decreases image resolution. This shows that noise cannot be reduced arbitrarily. An increased signal-to-noise ratio is beneficial for a reliable diagnosis and subsequent image processing, like registration or segmentation. Many different approaches for noise suppression in CT have been investigated. For example, iterative numerical reconstruction techniques optimizing statistical objective functions [10,16,15]. The main drawback of these approaches is the high computational complexity. Furthermore, several linear or nonlinear filtering methods for noise reduction in the sinogram [11, 12,8] or reconstructed images [20,17] have been proposed. The disadvantage of denoising in the sinogram-space is the low signal-to-noise level, what makes a structure-preserving denoising difficult. Reducing noise after reconstruction is challenging mainly due to the difficult noise properties in CT: after reconstruction the noise distribution is unknown and noise is non-stationary. Further, directed noise due to high attenuation along certain directions makes the differentiation between structures and noise more complicated. In [1] we suggested to analyze the correlations between the wavelet representations of separately reconstructed images in order to distinguish between structures and noise. This method allows an automatic adaptation to the locally varying noise power in CT. However, no anisotropic denoising can be performed with this approach. This paper presents a new wavelet-thresholding method for edge-preserving, anisotropic noise reduction in CT-images.

A very important requirement for any noise reduction in medical images is that all clinically relevant image content must be preserved. A common approach for edge-preserving noise reduction is wavelet thresholding, based on the work of Donoho and Johnstone [9]. The input image is decomposed into wavelet coefficients. Insignificant detail coefficients below a defined threshold are erased, but those with larger values are preserved. The noise suppressed image is obtained by an inverse wavelet transformation from the modified coefficients. The difficulty is to find a proper threshold, especially for noise of spatially varying power and directed noise, which is commonly present in CT-images. Choosing a very high threshold may lead to visible loss of image structures, but the effect of noise suppression may be in-

sufficient, if the chosen threshold was too low. Therefore, a reliable estimation of noise for threshold determination is one of the main issues.

We show that the position and orientation dependent noise power in CT can be estimated from two separately reconstructed images, which only differ with respect to image noise. Therefore, the denoising method adapts itself to the noise power and allows for the reduction of spatially varying and oriented noise.

This paper is an extension of our work presented in [2] and is organized as follows: In section 2, the different steps used in the noise reduction method are described in detail. Section 3 presents the experimental evaluation based on simulated, as well as real clinical data. In section 4 the main observations of the experiments are discussed. Finally, section 5 summarizes the results and draws conclusions.

2 Material and Methods

2.1 Overview

An overview of the noise reduction method is shown in Fig. 1. First, two images A and B are generated, which only differ with respect to image noise. In CT, this can be achieved by separate reconstructions from disjoint subsets of projections $\mathrm{P1} \subset \mathrm{P}$ and $\mathrm{P2} \subset \mathrm{P}$, with $\mathrm{P1} \cap \mathrm{P2} = \emptyset$, $|\mathrm{P1}| = |\mathrm{P2}|$ and $\mathrm{P} = \mathrm{P1} \cup \mathrm{P2}$ ($|\mathrm{P}|$ defines the number of samples in P). Different possibilities for acquiring P1 and P2 exist:

- The simplest possibility is to scan the object twice, one time shortly after another with the same scanning parameters, each at half of the overall dose. However, this only works as long as the patient does not move.
- The acquisition of the two subsets can also be done during one single scan by splitting the overall number of projections into two disjoint sets afterwards. More specifically, one image is reconstructed from the even and the other from the odd numbered projections [1]. Here, it must be ensured that the sampling is high enough for the separate reconstruction of both datasets within the desired field-of-view.
- A third possibility is to use a dual-source CT scanner, where two tubes and two detectors with an offset of 90 degrees can work in parallel [3]. The two source-detector-systems need to be concerted in order to show comparable, but statistically uncorrelated, noise characteristics. Further, the same scanning and reconstruction parameters should be used for both source-detector-systems. One image can then be reconstructed from the projections acquired at the first and the other from the projections acquired at the second detector. The two resulting images include the same ideal noise-free signal but different noise.

Each of the images is then decomposed by a two dimensional stationary wavelet transformation (SWT) [5]. After this linear transformation, four two-dimensional blocks of coefficients are available at each decomposition level for each image: the lowpass filtered approximation image C and three detail images W^{H}, W^{V} and W^{D} including high frequency structures in horizontal (H), vertical (V) and diagonal (D) direction, together with noise in the respective frequency bands. For more details on wavelet theory we refer to [18,23,7]. The computation of the differences between the detail coefficients of the two input images A and B shows just the noise in the respective frequency band and orientation. This will be described in the next section in greater detail. These noise images can be used for the estimation of the position and orientation dependent standard deviation of noise in A and B. From this estimation, a thresholding mask is computed and applied to the averaged detail coefficients of the input images. The computation of the inverse wavelet transformation from the modified coefficients results in a noise-suppressed image. This again corresponds to the reconstruction from the complete set of projections but with improved signal-to-noise ratio.

2.2 Threshold Determination

The two images A and B are reconstructed from disjoint subsets of projections, where noise between the projections can be assumed to be uncorrelated (see [13, 4] for more information about CT reconstruction and the propagation of noise from the projections to the reconstructed slices). Consequently, A and B only differ with respect to image noise, but include the same ideal noise-free signal:

$$A = S + N_A\,, \quad B = S + N_B\,, \tag{1}$$

where $S = \mathrm{E}(A) = \mathrm{E}(B)$ represents the ideal noise-free image (the statistical expectation E) and $N_A \neq N_B$ zero-mean noise ($\mathrm{E}(N_A) = \mathrm{E}(N_B) = 0$) included in image A and B, respectively. Noise in both images is non-stationary, and consequently the standard deviation of noise depends on the local position $\mathbf{x} = (x_1, x_2)$. The standard deviations at a given pixel position are approximately the same in both images:

$$\sigma_A(\mathbf{x}) \approx \sigma_B(\mathbf{x}), \tag{2}$$

because on average the same number of contributing quanta can be assumed. Noise between the projections P1 and P2 is uncorrelated and accordingly noise between the separately reconstructed images is uncorrelated, too, leading to the following covariance:

$$\mathrm{Cov}(N_A, N_B) = 0. \tag{3}$$

We are now interested in the noise variance in a linear combination L of A and B defined as:

$$L = g_1 A + g_2 B, \tag{4}$$

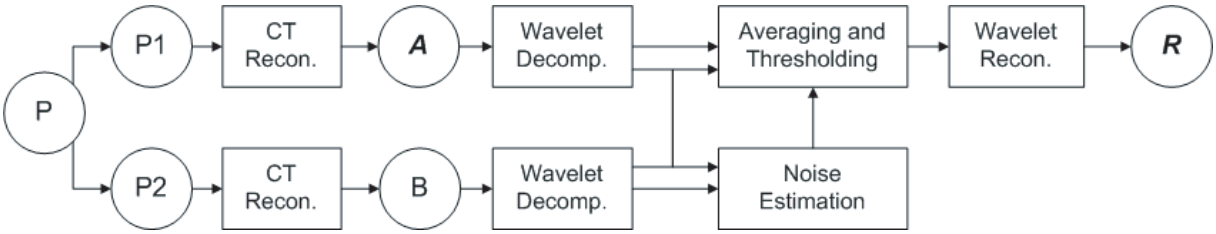

Fig. 1 Block diagram of the noise reduction method.

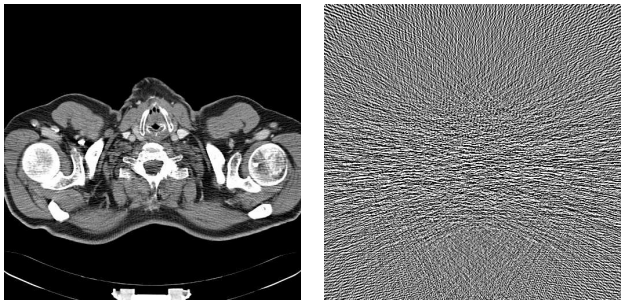

(a) Average M (b) Difference D

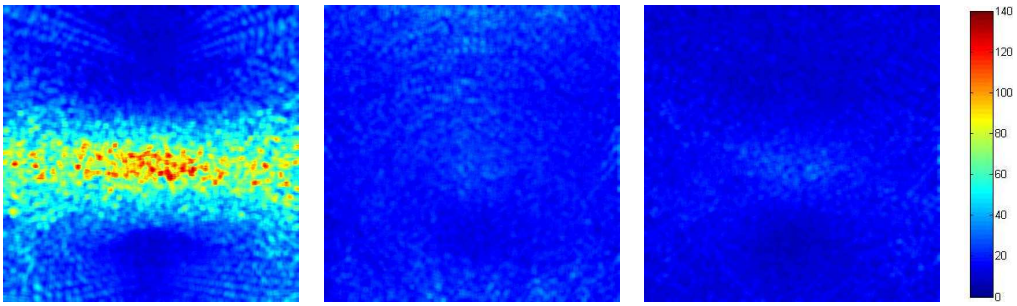

(c) Threshold τ_1^{H} (d) Threshold τ_1^{V} (e) Threshold τ_1^{D} (f)

Fig. 2 Example of orientation and position dependent threshold at the first decomposition level for thoracic image with strongly directed noise. The average of input images is shown in (a) and their difference in (b). The threshold images in horizontal (c), vertical (d) and diagonal (e) directions were computed with $k = 1.0$ and $s = 8$. The color-mapping is shown in (f).

with weights $g_1, g_2 \in \mathbb{R}$. For the variance of a linear combination of random variables the following holds [24]:

$$\sigma_L^2 = g_1^2\sigma_A^2 + g_2^2\sigma_B^2 + 2g_1g_2\mathrm{Cov}(A,B). \tag{5}$$

We can show that

$$\begin{aligned}\mathrm{Cov}(A,B) &= \mathrm{E}((A-\mathrm{E}(A))(B-\mathrm{E}(B))) \\ &= \mathrm{E}((A-S)(B-S)) \\ &= \mathrm{E}(N_A \cdot N_B) \\ &= \mathrm{Cov}(N_A,N_B) - \mathrm{E}(N_A)\mathrm{E}(N_B) \\ &= 0.\end{aligned} \tag{6}$$

Using eq. 2 and eq. 6, eq. 5 results in:

$$\sigma_L = \sqrt{g_1^2 + g_2^2}\,\sigma_A. \tag{7}$$

First of all, eq. 7 shows why the noise level in A and B is increased by a factor of $\sqrt{2}$ in comparison to the reconstruction from the complete set of projections or the average of the two input images $M = 0.5(A+B)$. Furthermore, it can be used for estimating noise in A and B and consequently in M from the difference of the input images. By the computation of the difference image

$$D = A - B = N_A - N_B\,, \tag{8}$$

we get a noise-image free of structures. Using eq. 7, we obtain that the standard deviations σ_A and σ_B of noise can be approximated from the standard deviation in the difference image σ_D by:

$$\sigma_A = \sigma_B = \frac{\sigma_D}{\sqrt{2}}\,. \tag{9}$$

Thus, the standard deviation of noise in the average image M results in:

$$\sigma_M = \frac{\sigma_A}{\sqrt{2}} = \frac{\sigma_D}{2}\,. \tag{10}$$

In order to compute a level and orientation dependent threshold for denoising in the wavelet domain, noise

in the different frequency bands and orientations should be estimated separately. Due to the known linearity of the wavelet transformation, the differences between the detail coefficients can also be directly used for noise estimation. At each decomposition level l the difference images

$$D_l^{\mathrm{H}} = W_{A,l}^{\mathrm{H}} - W_{B,l}^{\mathrm{H}}\,, \tag{11}$$
$$D_l^{\mathrm{V}} = W_{A,l}^{\mathrm{V}} - W_{B,l}^{\mathrm{V}}\,, \tag{12}$$
$$D_l^{\mathrm{D}} = W_{A,l}^{\mathrm{D}} - W_{B,l}^{\mathrm{D}} \tag{13}$$

between the detail coefficients are computed, where the subscripts A and B correspond to the two images and H, V and D again denote the horizontal, vertical and diagonal directions. These difference images are then used for the estimation of noise in the respective frequency band and orientation. In CT-images, the noise power is spatially varying. Therefore, noise estimation should be position dependent. For example, we estimate the standard deviation σ at decomposition level l in the horizontal direction according to:

$$\sigma_l^{\mathrm{H}}(\mathbf{x}) = \sqrt{\frac{1}{|\Omega_{\mathbf{x}}|}\sum_{\tilde{\mathbf{x}}\in\Omega_{\mathbf{x}}}(D_l^{\mathrm{H}}(\tilde{\mathbf{x}}))^2}, \tag{14}$$

within a local square pixel region $\Omega_{\mathbf{x}}$ centered around the current position $\mathbf{x} = (x_1, x_2)$ such that:

$$\Omega_{\mathbf{x}} = \left\{\tilde{\mathbf{x}}\middle|\, |x_j - \tilde{x}_j| \le s;\, \forall j = 1,2\right\}, \tag{15}$$

where the constant s defines the size of the pixel region and, thus, the number of pixels $|\Omega_{\mathbf{x}}|$ used for the local noise estimation. Analogously, we obtain the noise estimates for the vertical and diagonal directions. From the three standard deviation images σ_l^{H}, σ_l^{V} and σ_l^{D} we compute for all decomposition levels, orientation and position dependent thresholds according to:

$$\tau_l^{\mathrm{H}} = k\frac{\sigma_l^{\mathrm{H}}}{2} \tag{16}$$
$$\tau_l^{\mathrm{V}} = k\frac{\sigma_l^{\mathrm{V}}}{2}$$
$$\tau_l^{\mathrm{D}} = k\frac{\sigma_l^{\mathrm{D}}}{2}$$

The constant k controls the amount of noise suppression. With increasing k more noise is removed. In Fig. 2(c)-2(e) the thresholds computed with $s = 8$ for the first decomposition level in the horizontal, vertical and diagonal directions are shown for a thorax-slice (see average of input images in Fig. 2(a)) with strongly directed noise (see difference of input images in Fig. 2(b)).

2.3 Averaging and Thresholding

The computed thresholds from eq. (16) are then applied to the averaged wavelet coefficients of the input images:

$$W_{M,l}^{\mathrm{H}} = 0.5\cdot(W_{A,l}^{\mathrm{H}} + W_{B,l}^{\mathrm{H}}), \tag{17}$$
$$W_{M,l}^{\mathrm{V}} = 0.5\cdot(W_{A,l}^{\mathrm{V}} + W_{B,l}^{\mathrm{V}}),$$
$$W_{M,l}^{\mathrm{D}} = 0.5\cdot(W_{A,l}^{\mathrm{D}} + W_{B,l}^{\mathrm{D}}).$$

We perform a *hard* thresholding, meaning that all averaged coefficients with an absolute value below the threshold are set to zero and values above are kept unchanged:

$$W_{R,l} = \begin{cases} W_{M,l}, & \text{if } |W_{M,l}| \ge \tau_l, \\ 0, & \text{else.} \end{cases} \tag{18}$$

The approximation coefficients $C_{A,l_{\max}}$ and $C_{A,l_{\max}}$ of A and B at the maximum decomposition level $l_{\max}$ are simply averaged:

$$C_{R,l_{\max}} = 0.5\cdot(C_{A,l_{\max}} + C_{B,l_{\max}}). \tag{19}$$

The final noise suppressed image is computed by an inverse wavelet transformation from the averaged and weighted wavelet coefficients of the input images.

3 Results

3.1 Noise and Resolution

In evaluating the performance of the noise reduction method, mainly two aspects are of interest: the amount of noise reduction and, even more importantly, the preservation of anatomical structures. Therefore, we investigated the influence of the noise suppression method to the standard deviation of noise and image resolution.

For our experiments we used reconstructions from a simulated elliptical water phantom ($dx = 20\,\mathrm{cm}$, $dy = 10\,\mathrm{cm}$), with an embedded, quartered cylinder ($r = 6\,\mathrm{cm}$) with a contrast of 100 HU. For this test, P1 and P2 were simulated independently, corresponding to two consecutive scans or the acquisition with a dual-source-scanner. All simulations were performed with the *DRASIM* software package provided by Karl Stierstorfer [21]. The advantage of simulations is that in addition to noisy projections (with Poisson distributed noise according to quantum statistics), ideal, noise-free data can also be produced. All slices are of size 512×512 and were reconstructed using the weighted filtered backprojection [22] within a field of view of 20 cm using a sharp Shepp-Logan filtering kernel. This results in an average pixel noise of approximately 22.4 HU in the homogeneous image region in the reconstruction from the complete set of projections. The standard deviation of noise in the separately reconstructed images is about $\sqrt{2}$ times higher.

All images were denoised with the proposed method up to the fourth decomposition level of a Haar-SWT.

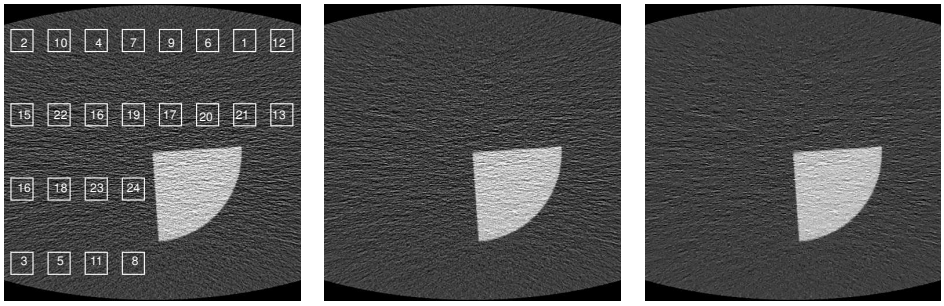

(a) Original noisy phantom ($k = 0$) (b) *ANESWT* with $k = 1.0$ (c) *ANESWT* with $k = 1.5$

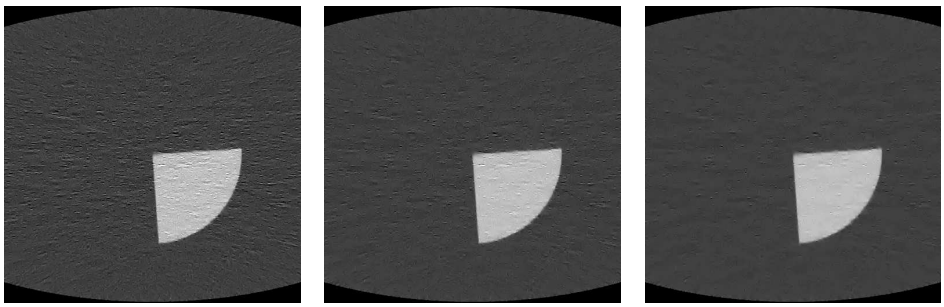

(d) *ANESWT* with $k = 2.0$ (e) *ANESWT* with $k = 2.5$ (f) *ANESWT* with $k = 3.0$

Fig. 3 Phantom used for noise and resolution evaluation. (a) Original noisy phantom, where regions used for noise evaluation are marked. (b)-(f) Denoised images achieved with proposed method (*ANESWT*) with different values of parameter k controlling the amount of noise suppression. Center and window settings used for displaying CT-images: center=50, window=200.

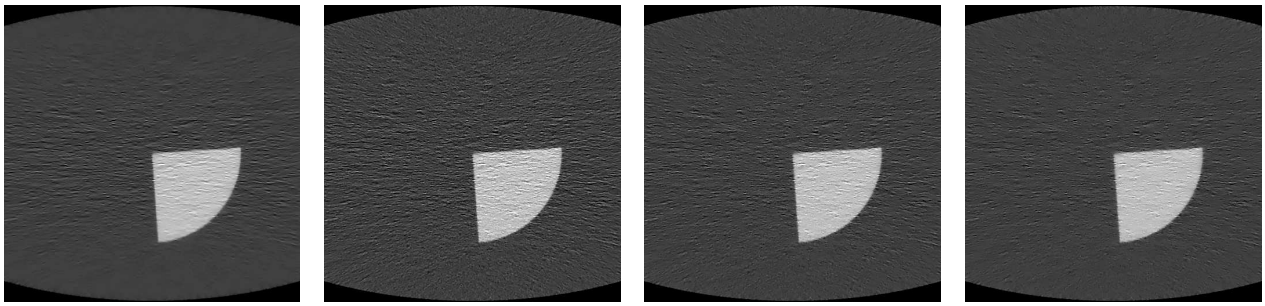

(a) *STSWT* (b) *CASWT* with $p = 1.0$ (c) *CASWT* with $p = 2.0$ (d) *CASWT* with $p = 3.0$

Fig. 4 Denoising results achieved with standard wavelet thresholding (*STSWT*) (a) and correlation analysis based wavelet denoising (CASWT) (b)-(d) for different values of parameter p controlling the amount of noise suppression. Center and window settings used for displaying CT-images: center=50, window=200.

We used $s = 4$ for the pixel region defined in equation (15) and compare the results for different values of $k \in \{1, 1.5, 2, 2.5, 3\}$ regulating the amount of noise suppression. We compared the proposed method with a standard wavelet thresholding method that is not specially adapted for the use in CT. We used the *SWT Denoising 2D* tool from the Matlab wavelet toolbox [19]. For denoising in Matlab, we used a *Balance Sparsity-Norm* hard thresholding method with a non-white-noise model and again four levels of a Haar-SWT. Further, we compared proposed method with another wavelet denoising method for edge-preserving noise reduction in CT, as presented in [1]. The weights at each decomposition level were gained from a correlation analysis between the approximation images of the previous decomposition level. We used again four decomposition levels of a Haar-SWT and computed the correlation within neighborhoods of 5×5 pixels around the corresponding position. The amount of noise suppression was controlled by the power within the weighting function, denoted by parameter
$p \in \{1, 1.5, 2, 2.5, 3\}$. In the following we use the abreviation *STSWT* for the standard thresholding, *CASWT* for the correlation analysis based denoising method, and *ANESWT* for the proposed adaptive noise estimation based method.

In Fig. 3 the used noisy phantom together with the denoised images achieved with *ANESWT* for different

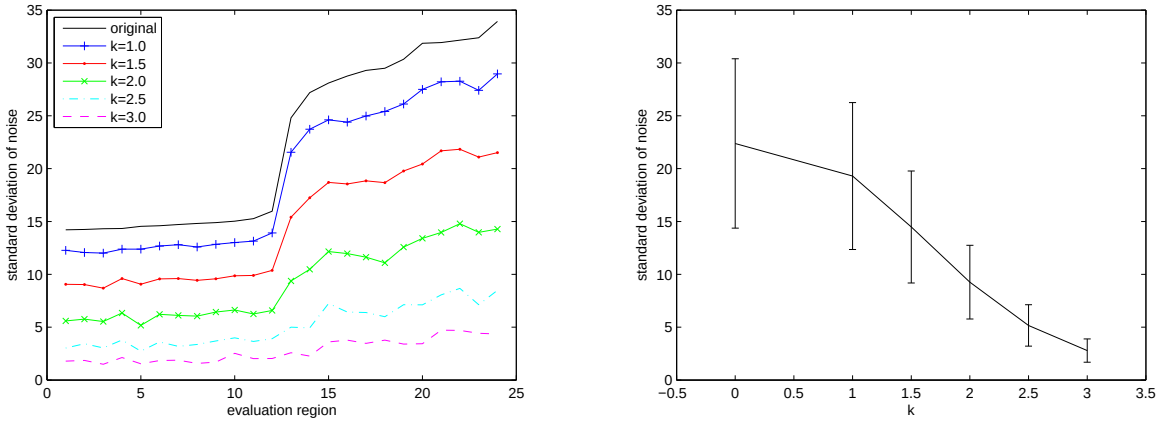

(a) Standard deviation of noise (b) Mean noise and standard deviation between regions

Fig. 5 Noise evaluation for *ANESWT* in different pixel regions marked in Fig. 3(a). (a) Comparison of standard deviation of noise in different pixel regions for different values of k. (b) Mean standard deviation of noise of all pixel regions together with standard deviation between different pixel regions for different values of k.

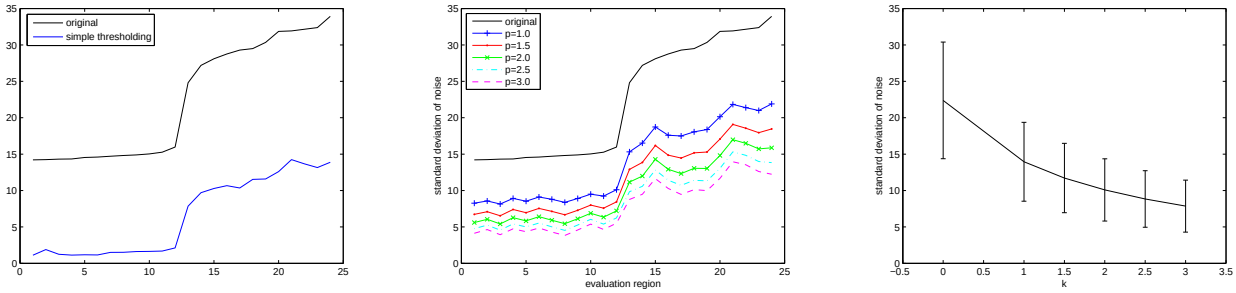

(a) Standard deviation of noise - *STSWT* (b) Standard deviation of noise - *CASWT* (c) Mean noise and standard deviation between regions - *CASWT*

Fig. 6 Noise evaluation for *STSWT* (a) and CASWT (b) and (c). The same pixel regions were used, as marked in Fig. 3(a). (a) Standard deviation of noise in different pixel regions, (b) comparison of standard deviation of noise in different pixel regions for different values of p. (b) Mean standard deviation of noise of all pixel regions together with standard deviation between different pixel regions for different values of p.

values of k are shown. Due to the eccentricity of the used phantom, we got directed noise, pointing out in the direction of highest attenuation, as can be seen in the original noisy image in Fig. 3(a). For better comparison, the denoising results achieved with *STSWT* and *CASWT* for different values of p are presented in Fig. 4. In order to compare the noise homogeneity before and after denoising, we evaluated the standard deviations of noise in 24 homogeneous image regions of 40×40 pixels as marked in Fig. 3(a). The standard deviations of noise in the different pixel regions are plotted in Fig. 5(a) for the original and the denoised images using *ANESWT*. The pixel regions are numbered incrementally according to their standard deviation of noise in the original image. It can be seen that with increasing k stronger noise suppression is achieved. Furthermore, it can be seen that, with increasing k, noise between the different evaluation regions becomes more homogeneous. This is even clearer in Fig. 5(b), where the average standard deviations of noise from all evaluation regions are plotted for the different values of k ($k = 0$ denotes the original image), together with the standard deviations between the 24 evaluation regions. As Fig. 5(b) shows, with increasing k not only the average noise in the image is reduced, but also the standard deviation between the pixel regions is decreased.

Fig. 6(a) shows the noise evaluation for *STSWT*. In all pixel regions the standard deviation of noise was decreased. However, it can be seen, that the algorithm does not adapt to the noise level in the image. Regions with a higher noise level are not stronger denoised. Fig. 6(b) shows the noise evaluation for *CASWT*. The average standard deviation of noise together with the standard deviation between the different pixel regions is shown in Fig. 6(c). With increasing parameter p a stronger noise suppression is achieved. The direct comparison of the standard deviations of noise in the different pixel regions between *ANESWT* and *CASWT* shows that a compara-

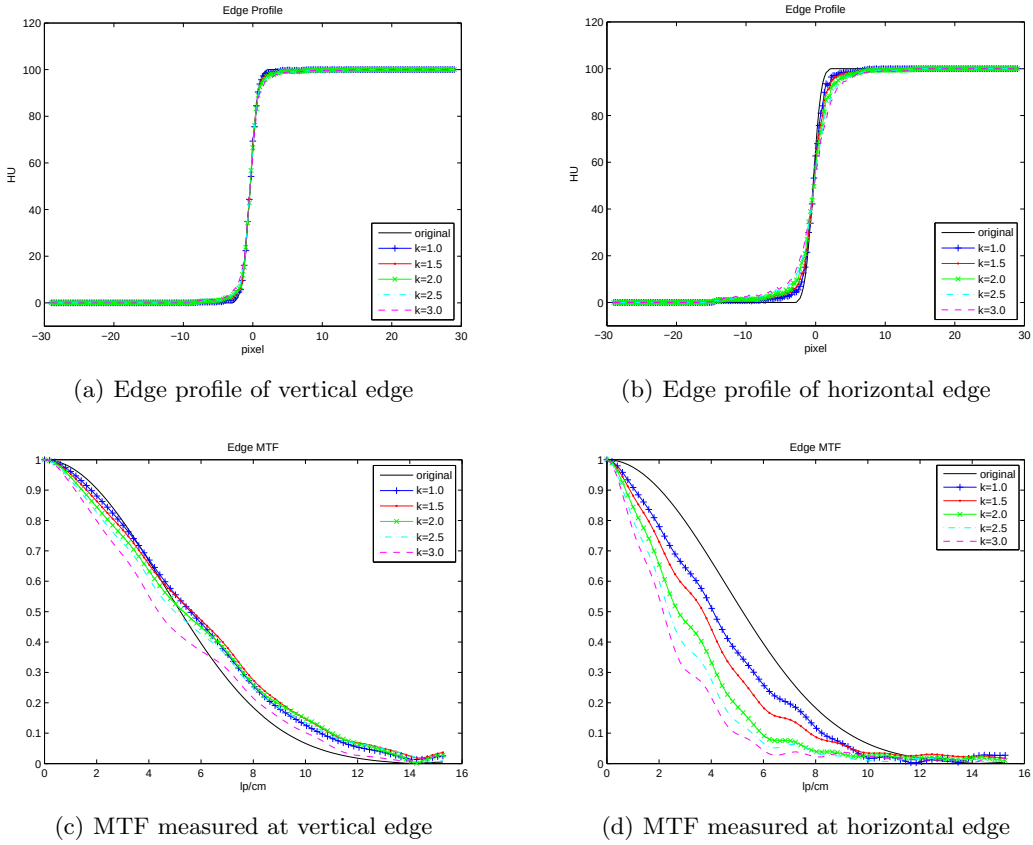

(a) Edge profile of vertical edge

(b) Edge profile of horizontal edge

(c) MTF measured at vertical edge

(d) MTF measured at horizontal edge

Fig. 7 Evaluation of image resolution for *ANESWT*. Average edge profiles of the vertical (a) and horizontal (b) edge and MTFs of vertical (c) and horizontal (d) edge are compared for different values of k.

ble noise suppression in pixel regions 1-12 is e.g. achieved for $k = 2.0$ and $p = 2.0$. In contrast to that, the average noise suppression in pixel regions 13-24 achieved with $k = 2.0$ corresponds to that of $p = 2.5$. *ANESWT* reduces more noise in regions with strong directed noise. Consequently, a lower standard deviation between the different pixel regions is achieved.

For evaluating image resolution, we used a standard measurement for resolution in CT. The modulation transfer function (MTF) (see e.g. [4]) indicates how many line pairs per cm (lp/cm) can be distinguished. It is possible to determine the local MTF directly from the edge in an image. For this purpose, we manually selected a fixed region around the horizontal or vertical edge of the quartered cylinder. The slight tilt of the edge allows a higher sampling of the edge profile, which is additionally averaged along the edge. The derivation of the edge profile leads to the line-spread function (LSF). The Fourier transformation of the LSF results in the MTF, which is additionally normalized so that MTF(0) = 1. Reliable measurements of the MTF from this *edge technique* can only be achieved if the contrast of the edge is much higher than the pixel noise in the images [6]. This can be easily avoided by applying the computed weights at each decomposition level to the wavelet coefficients of the ideal noise-free image and computing the inverse transformation. This has the effect of making the influence of the weighting to the real signal directly visible. The local MTF can then be computed at the edge in the processed noise-free image. In Fig. 7 the edge profiles of the vertical and horizontal edge and the corresponding MTFs can be seen. In Fig. 7(a) and 7(c) it can be seen that the vertical edge was very well preserved. Image resolution at the vertical edge could even be improved. In contrast to that, a slight blurring is noticeable at the horizontal edge, as can be seen in Fig. 7(b) and 7(d). In Fig. 8 the resolution evaluations performed for *CASWT* are shown. Here, it can be observed that there is nearly no difference with respect to edge-preservation for the horizontal and vertical edge.

3.2 Example Images

In Fig. 9(d) and 9(f), zoomed-in noise-suppressed results from the proposed method applied to a thoracic image (see Fig. 2(a)) are shown for two different settings of k. The two input datasets A and B were generated by separate reconstructions from even and odd numbered projections. The difference images (Fig. 9(e), 9(g)) between the denoised and average of input images (Fig. 9(a)) are also displayed. The images are compared to the denoising

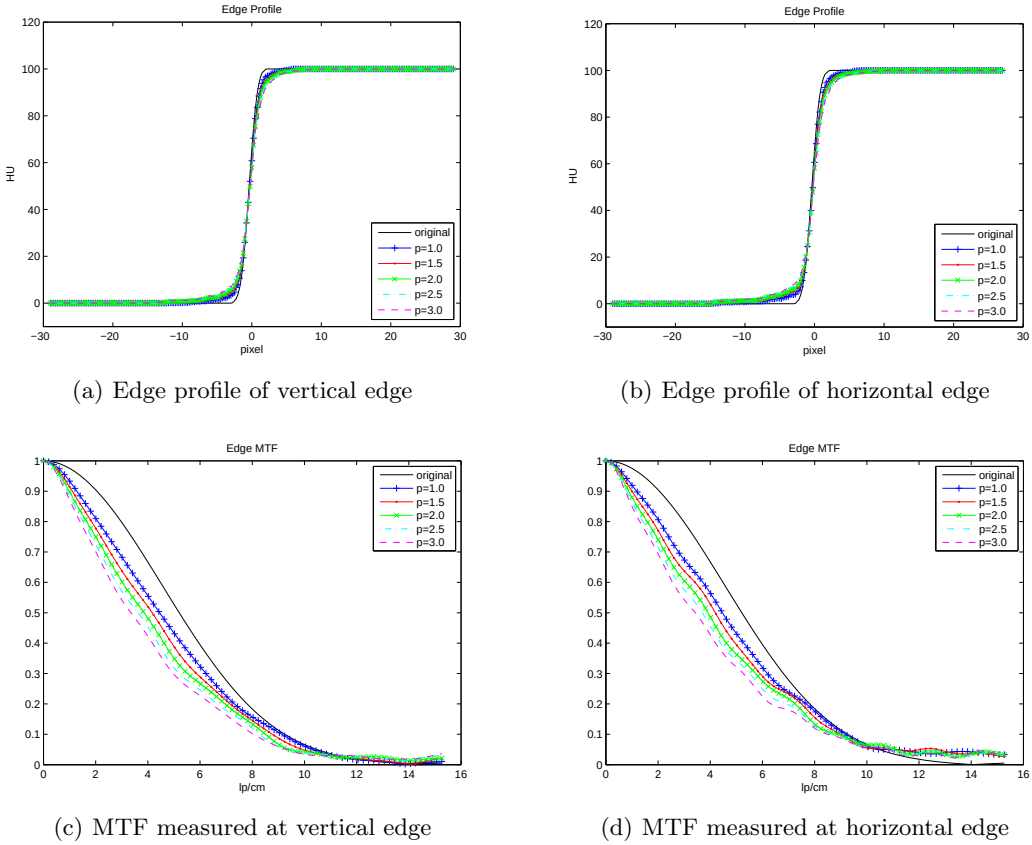

(a) Edge profile of vertical edge

(b) Edge profile of horizontal edge

(c) MTF measured at vertical edge

(d) MTF measured at horizontal edge

Fig. 8 Evaluation of image resolution for *CASWT*. Average edge profiles of the vertical (a) and horizontal (b) edge and MTFs of vertical (c) and horizontal (d) edge are compared for different values of p.

result achieved with the *SWT De-noising 2D* tool from the Matlab wavelet toolbox [19] (see Fig. 9(b) and 9(c)). All computations were performed using a Haar wavelet decomposition up to the fourth decomposition level. For denoising in Matlab, we used a *Balance Sparsity-Norm* hard thresholding method with a non-white-noise model.

The difference image in Fig. 9(c) shows that standard wavelet denoising methods reduce noise in the images, but also blur edges. The reason for this is that no reliable noise estimation is possible if just one CT-image is available. In contrast, the proposed method adapts itself to the spatially varying noise power in the different frequency bands and orientations and, therefore, performs much better especially in images with directed noise.

4 Discussion

The experiments in the previous section showed that standard denoising techniques like *STSWT* lead to unconvincing results if they are applied to CT images. The reason for this can be found in the difficult noise properties in CT. The noise distribution after reconstruction is not known, noise is non-stationary and directed noise may be present. This makes the distinction between real structures and noise more complicated. The presented examples, where *STSWT* was applied to CT slices with directed noise, clearly showed that in regions of higher noise level noise still remains in the image, while other regions already get blurred.

The *CASWT*, another wavelet based method for noise suppression on CT data, showed that an adaptation to the noise level is performed. The method adapts itself to the noise level of the input data by computing the local correlations between the wavelet representations of two separately reconstructed CT images. At each decomposition level, one weighting image is computed. This is applied equally to the different directions. Therefore, this method does not allow an anisotropic. In images with strong directed noise, a higher noise suppression always influences the resolution in horizontal and vertical direction in the same way.

The proposed method adapts itself to the local and orientation dependent noise power in CT. In contrast to *CASWT*, the proposed *ANESWT* performs an anisotropic noise reduction. Noise is estimated separately within the different frequency bands and orientations of the wavelet decomposition. The thresholds used for denoising are chosen in adaptation to the local noise estimates. Consequently, locally varying and also directed noise can be removed efficiently. The evaluation of noise in different pixel regions showed that stronger denoising

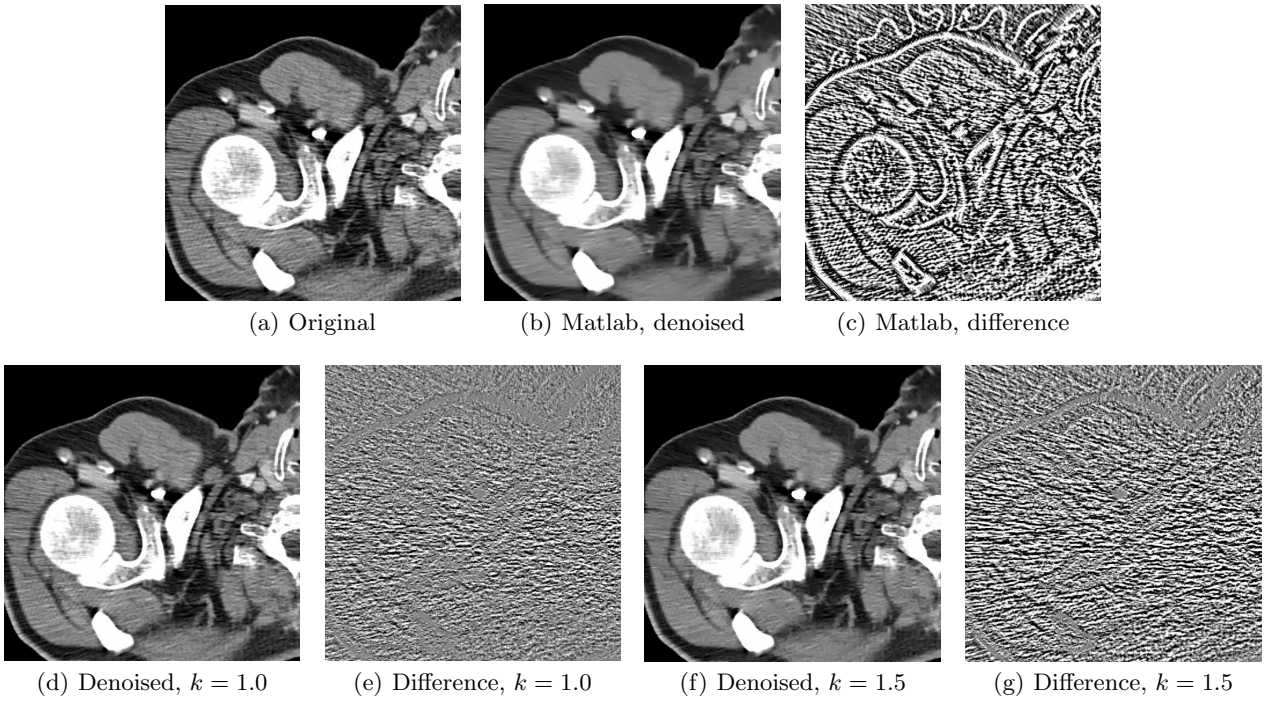

(a) Original (b) Matlab, denoised (c) Matlab, difference

(d) Denoised, $k = 1.0$ (e) Difference, $k = 1.0$ (f) Denoised, $k = 1.5$ (g) Difference, $k = 1.5$

Fig. 9 Denoising result of the proposed method (d),(f) in comparison to standard wavelet thresholding method from the Matlab wavelet toolbox (b) in pixel region taken from a thorax-slice with strongly directed noise (a). The corresponding difference images to the original (a) are displayed in (c),(e) and (g). Center and window settings used for displaying CT-images: center=50, window=400. Center and window settings used for displaying difference images: center=0, window=30.

is performed where stronger directed noise is present. This has the effect that not only the overall noise power is reduced, but also the standard deviation between the different evaluation regions is decreased. Thus, the homogeneity of noise within the image is improved. The anisotropic behavior of the proposed method can also be observed in the evaluation of resolution. With *ANESWT*, stronger smoothing is performed orthogonal to the direction of the directed noise. This is the reason why with increasing k stronger blurring is visible at the horizontal than at the vertical edge. In comparison to *CASWT* the blurring at the horizontal edge is slightly increased. However, the vertical edge is nearly perfectly preserved, also at high noise reduction rates. The anisotropic behavior is beneficial, especially in cases where directed noise due to high attenuation along certain directions is present.

The experiments performed on clinical data showed that directed noise could be removed without noticeable loss of resolution with the new denoising approach. Especially, the difference images between the original and denoised images show that nearly no structure was removed. Further, it can be seen that noise along edges could also be removed. The comparison to *STSWT* applied to clinical data again showed that no reliable estimation of locally-varying and directed noise can be achieved if just one input image is available. In the example shown, noise was over-estimated resulting in strong blurring at the edges.

The proposed method is computationally efficient. The cost for reconstructing the two datasets A and B separately corresponds a reconstruction from the complete set of projections. Two reconstructions each with only half the number of projections are needed, if only the even or odd numbered projections are used respectively. Otherwise, if the object is scanned twice or a dual-source-scanner is used two complete reconstructions are needed. The denoising process can be computed efficiently. There are two wavelet decompositions and one inverse wavelet transformation to be computed. The complexity of the SWT is linear with the number of pixels. All computations needed for weighting the coefficients are performed within local neighborhoods. Thus, the method is well suited for parallel computation.

5 Conclusions

In this paper, we proposed a new, robust and efficient wavelet domain denoising technique for the suppression of pixel noise in CT-images. The separate reconstructions from disjoint subsets of projections allows the generation of images which only differ with respect to image noise but include the same ideal noise-free signal. We showed that noise can be locally estimated in the different frequency bands and orientations of the wavelet transformation, based on the difference between the wavelet coefficients of the two separate reconstructions. With

this technique, position and orientation adaptive thresholds can be computed at each decomposition level for noise reduction. The evaluation on simulated as well as on real clinical CT data showed that the method adapts itself to the locally varying noise power and can also deal with difficult noise conditions like directed noise. The comparison of our proposed method to a standard wavelet denoising method and another wavelet denoising method for CT showed that better edge-preservation can be achieved and homogeneity of noise within the image can be improved.

Acknowledgement

The authors would like to thank Holger Kunze, Karl Stierstorfer and Elli Angelopoulou for helpful suggestions and discussions. Further, the authors gratefully acknowledge the finical support by Siemens Medical Solutions, the international Max-Planck research school (IMPRS) on optics and imaging and the school in advanced optic technologies (SAOT).

References

1. Borsdorf, A., Raupach, R., Hornegger, J.: Wavelet based Noise Reduction by Identification of Correlation . In: K. Franke, K. Müller, B. Nickolay, R. Schäfer (eds.) Pattern Recognition (DAGM 2006), Lecture Notes in Computer Science , vol. 4174, pp. 21–30. Springer, Berlin (2006)
2. Borsdorf, A., Raupach, R., Hornegger, J.: Separate CT-Reconstruction for Orientation and Position Adaptive Wavelet Denoising . In: A. Horsch, T. Deserno, H. Handels, H. Meinzer, T. Tolxdoff (eds.) Bildverarbeitung fr die Medizin 2007 , pp. 232–236. Springer, Berlin (2007)
3. Bruder, H., Stierstorfer, K., McCullough, C., Raupach, R., Petersilka, M., Grasruck, M., Suess, C., Ohnesorge, B., Flohr, T.: Design considerations in cardiac CT. In: M. Flynn, J. Hsieh (eds.) Medical Imaging 2006: Physics of Medical Imaging. Proceedings of the SPIE , vol. 6142, pp. 151–163 (2006)
4. Buzug, T.: Einführung in die Computertomographie. Springer-Verlag, Berlin Heidelberg (2004)
5. Coifman, R.R., Donoho, D.L.: Translation-invariant denoising. In: Lecture Notes in Statistics: Wavelets and Statistics, vol. 103, pp. 125–150 (1995)
6. Cunningham, I.A., Reid, B.K.: Signal and noise in modulation transfer function determinations using the slit, wire, and edge techniques. Medical Physics **19**(4), 1037–1044 (1992)
7. Daubechies, I.: Ten Lectures on Wavelets. Society for Industrial and Applied Mathematics, Philadelphia (1992)
8. Demirkaya, O.: Reduction of noise and image artifacts in computed tomography by nonlinear filtration of projection images. In: M. Sonka, K.M. Hanson (eds.) Proc. SPIE Vol. 4322, p. 917-923, Medical Imaging 2001: Image Processing, pp. 917–923 (2001)
9. Donoho, D.L., Johnstone, I.M.: Ideal spatial adaptation by wavelet shrinkage. Biometrika **81**(3), 425–455 (1994)
10. Fessler, J., Ficaro, E., Clinthorne, N., Lange, K.: Grouped-coordinate ascent algorithms for penalized-likelihoodtransmission image reconstruction. IEEE Trans Med Imaging **16**(2), 166–175 (1997)
11. Hsieh, J.: Adaptive streak artifact reduction in computed tomography resulting from excessive x-ray photon noise. Medical Physics **25**(11), 2139–2147 (1998)
12. Kachelrieß, M., Watzke, O., Kalender, W.A.: Generalized multi-dimensional adaptive filtering for conventional and spiral single-slice, multi-slice, and cone-beam CT. Medical Physics **28**(4), 475–490 (2001)
13. Kak, A., Slanely, M.: Principles of Computerized Tomographic Imaging. Society for Industrial and Applied Mathematics (2001). Http://www.slaney.org/pct/pct-toc.html
14. Kalender, W.: Computed Tomography. Publics MCD Werbeagentur GmbH, Munich (2000)
15. La Rivire, P., Bian, J., Vargas, P.: Penalized-likelihood sinogram restoration for computed tomography. IEEE Trans Med Imaging **25**(8), 1022–1036 (2006)
16. Li, T., Li, X., Wang, J., Wen, J., Lu, H., Hsieh, J., Liang, Z.: Nonlinear sinogram smoothing for low-dose X-ray CT. IEEE Transactions on Nuclear Science **51**(5), 2505–2512 (2004)
17. Lu, H., Li, X., Li, L., Chen, D., Xing, Y., Hsieh, J., Liang, Z.: Adaptive noise reduction toward low-dose computed tomography. In: M.J. Yaffe, L.E. Antonuk (eds.) Medical Imaging 2003: Physics of Medical Imaging., *Presented at the Society of Photo-Optical Instrumentation Engineers (SPIE) Conference*, vol. 5030, pp. 759–766 (2003)
18. Mallat, S.G.: A theory for multiresolution signal decomposition: The wavelet representation. IEEE Transactions on Pattern Analysis and Maschine Intelligence **11**(7), 674–693 (1989)
19. Mathworks Inc.: Wavelet Toolbox (2006). http://www.mathworks.com/products/wavelet/
20. Rust, G.F., Aurich, V., Reiser, M.: Noise/dose reduction and image improvements in screening virtual colonoscopy with tube currents of 20 mAs with nonlinear Gaussian filter chains. In: A.V. Clough, C.T. Chen (eds.) Proc. SPIE Vol. 4683, p. 186-197, Medical Imaging 2002: Physiology and Function from Multidimensional Images, Anne V. Clough; Chin-Tu Chen; Eds., pp. 186–197 (2002)
21. Stierstorfer, K., Flohr, T., Bruder, H.: Segmented multiple plane reconstruction: A novel approximate reconstruction scheme for multi-slice spiral CT. Physics in Medicine and Biology **47**(4), 2571–2581 (2002)
22. Stierstorfer, K., Rauscher, A., Boese, J., Bruder, H., Schaller, S., Flohr, T.: Weighted FBP - a simple approximate 3DFBP algorithm for multislice spiral CT with good dose usage for arbitrary pitch. Physics in Medicine and Biology **49**(11), 2209–2218 (2004)
23. Strang, G., Nguyen, T.: Wavelets and Filter Banks. Wellesley- Cambridge Press (1996)
24. Weisstein, E.W.: Variance (2006). From MathWorld - A Wolfram Web Resource, http://mathworld.wolfram.com/Variance.html